Journal of Microscopy, Vol. 187, Pt 1, July 1997, pp. 1–7.
Received 23 April 1997; accepted 14 May 1997

SHORT COMMUNICATION

Far-field fluorescence microscopy with three-dimensional resolution in the 100-nm range

S. W. HELL,* M. SCHRADER & H. T. M. VAN DER VOORT†
**High Resolution Optical Microscopy, Max-Planck-Institute for Biophysical Chemistry, Göttingen, Germany, and Department of Medical Physics and Chemistry, University of Turku, Finland*
†Scientific Volume Imaging BV, Hilversum, the Netherlands

Key words. 4Pi confocal microscopy, fibroblast, fluorescence, point spread function, resolution, restoration, superresolution, two-photon.

Summary

We report three-dimensional (3D) microscopy with nearly isotropic resolution in the $\lambda/5 - \lambda/10$ range. Our approach combines 4Pi-confocal two-photon fluorescence microscopy with image restoration. The 3D resolution is demonstrated with densely clustered beads as well as with F-actin fibers in mouse fibroblast cells. A comparison with unrestored two-photon confocal images reveals a total reduction of the uncertainty volume up to a factor of 15.

Introduction

More than a century ago, Abbe's theory of image formation highlighted the difficulties in improving the resolution of a far-field light microscope (Abbe, 1873). Since then, concepts such as electron and near-field light microscopy have evolved, which have either abandoned the use of light, or rely on a surface–tip interaction (Marti & Amrein, 1993). Unfortunately, these microscopes require detrimental specimen preparation to obtain a three-dimensional (3D) image. While confocal (Wilson, 1990) and multiphoton microscopes (Denk *et al.*, 1990; Hell *et al.*, 1996; Wokosin *et al.*, 1996; Schrader *et al.*, 1997) can image transparent specimens in 3D, these microscopes could not significantly change the resolution issue. The resolution of confocal and multiphoton microscopes does not exceed $\lambda/3$ and λ in the lateral and axial directions, respectively, with λ denoting the wavelength of light. The poorer axial resolution also overemphasizes structures orientated along the optic axis, i.e. objects which lie along the optic axis appear brighter than identical objects which lie in the lateral plane. Therefore, one of the major aims in light microscopy is to achieve isotropic 3D imaging at higher resolution.

Increasing the resolution is challenging, as the limits are rooted in the wave nature of light. Despite this, several approaches have been proposed, with the most popular being the computational restoration of the image with the point-spread-function (PSF) of the microscope (Castleman, 1979; Agard & Sedat, 1983). Progress has been made in the restoration of conventional (Carrington *et al.*, 1995), confocal and two-photon images (Kano *et al.*, 1996), but the axial resolution has not been improved beyond about 300–400 nm in a biological specimen, thus leaving the problem of nonisotropy unsolved. An enhancement of axial resolution has been reported by standing wave microscopy (Bailey *et al.*, 1993), but this is not a 3D method and often requires the objects to be thin, of the order of λ. Confocal theta microscopy (Stelzer & Lindek, 1994) uses two orthogonal lenses to provide isotropic resolution. However, the physical size of the objectives dictates that those used in theta microscopy are of relatively low numerical aperture. This means that whilst the resolution of this configuration is approximately isotropic it is not as high as the 3D resolution achieved with high-numerical-aperture objectives in a confocal configuration (Sheppard, 1995). Recently, various offset beam scanning microscopes have been described (Hell, 1994; Hell & Wichmann, 1994; Vaez-Iravani & Kavaldjiev, 1995; Müller & Brakenhoff, 1996). These intriguing techniques are expected to play a role in the future, but require further technical development.

4Pi-confocal microscopy (Hell, 1990), on the other hand, increases the axial resolution by extending the aperture with two opposing high-aperture lenses. In 4Pi-confocal microscopy of type A this is achieved by illuminating both lenses with coherent light, so that constructive interference

Correspondence to S.W. Hell, email: shell@gwdg.de

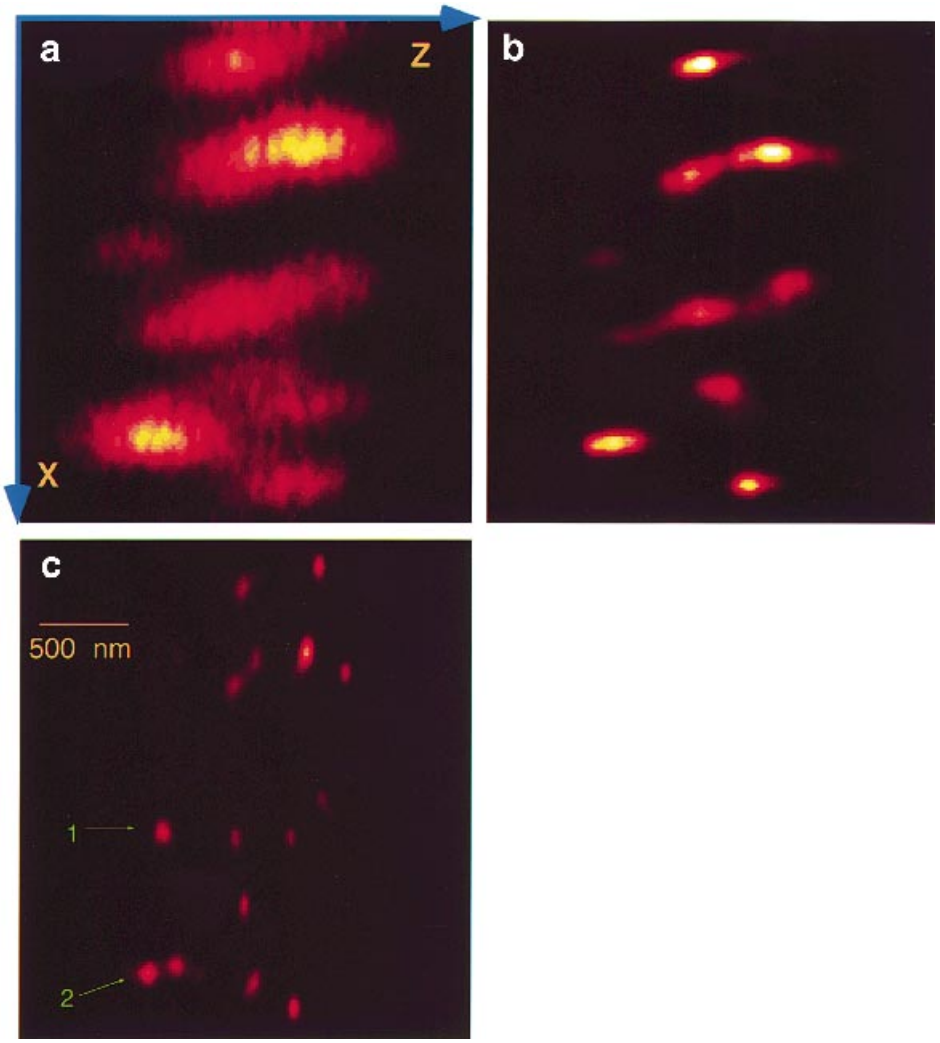

Fig. 1. Confocal (a), restored confocal (b) and restored 4Pi-confocal (c) two-photon *xz*-images of clustered beads. The comparison between (a) and (c) reveals a three- and seven-fold improvement of lateral and axial resolution in restored 4Pi-confocal microscopy. The *xz*-images are part of a 3D image of 12 *xz*-slices, all of which show similar results.

of the focused wavefronts results in an axial PSF that is 4·5 times sharper than that of a confocal microscope. This mode of excitation gives rise to a prominent lobe above and below the focal plane. Multiphoton excitation of the dye reduces the relative strength of the lobes. The higher order dependence of the fluorescence on the excitation intensity, and the axial discrimination of the confocal pinhole, keeps the intensity of the lobes to about 30–45% of the main focal maximum for two-photon excitation (Hell & Stelzer, 1992; Schrader & Hell, 1996). Importantly, two-photon 4Pi-confocal PSF approximately follows a cubic-law intensity dependence, with two orders stemming from the two-photon transition and another order from the confocal discrimination. Thus, a spatially defined focus is achieved, making two-photon 4Pi-confocal microscopy ideally suitable for restoration.

Material and methods

The success of any restoration depends critically on the signal-to-noise ratio (SNR) of the image. Our images feature a high SNR which is due to the combination of object scanning with avalanche photodiode detection (Kano *et al.*, 1996; Schrader *et al.*, 1996). The samples were scanned with a piezoelectric stage (Melles Griot, Cambridge, U.K.) at a typical pixel dwell time of 2 ms. The quantum efficiency of the detector (SPCM-131, EG&G Canada) was 40–70% in the green–red wavelengths regime. 3D-piezo-scanning of the sample ensured a high translation invariance of the PSF, which is another prerequisite for efficient restoration. Two-photon excitation was performed at about 810 nm using a mode-locked titanium–sapphire laser (Mira 900F, Coherent). We used standard oil immersion lenses with a

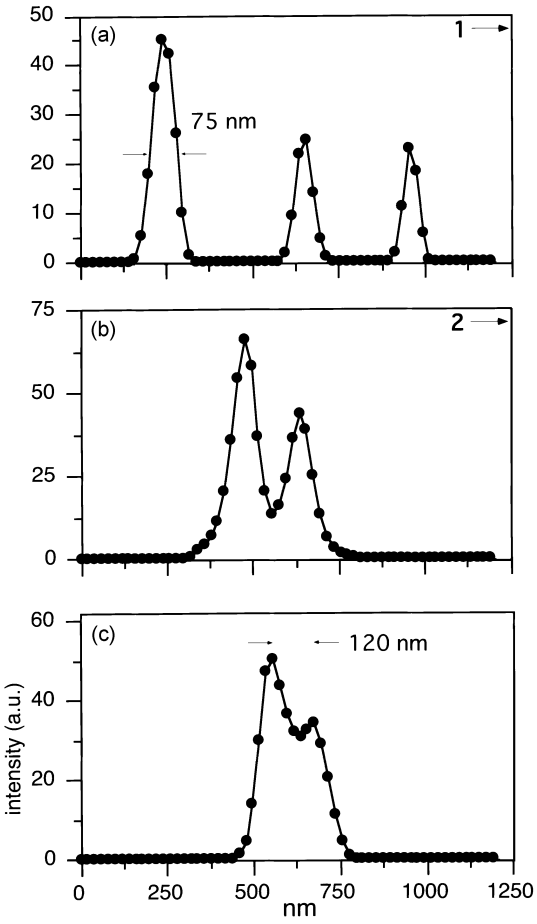

Fig. 2. Image profiles of adjacent beads of Fig. 1; (a) in direction of arrow 1, (b) of arrow (2) and (c) in a further layer of the 3D image, as encountered in the restored 4Pi-confocal recording. Profiles (b) and (c) reveal the ability to fully distinguish diameter 115 nm beads at closest proximity. Note the dense pixelation in the data.

numerical aperture of 1·4 (Leica PL Apo 100×). The samples were mounted between two coverslips to enable illumination from both sides. The confocal and the 4Pi data were recorded with the same average power, i.e. 1 mW for the cells and 0·5 mW for the beads. These power levels are considerably lower than the power required for saturation of the dye through ground state depletion (Denk *et al.*, 1990). The standard confocal images were obtained by blocking one of the lenses and then doubling the power of the remaining beam, so that the same illumination dose was used in the confocal and 4Pi-confocal recordings. The fluorescence light was filtered through a short-pass dichroic mirror and 2-mm-thick coloured glass (BG39, Schott) placed between the pinhole and the detector. The alignment of the 4Pi-confocal microscope and the adjustment of the phase is accomplished by imaging a single bead or F-actin fibre (Schrader & Hell, 1996).

The PSFs of the two-photon confocal and 4Pi-confocal microscope were extracted from images of isolated fluorescent beads. Ideally, the microscope PSF is measured by imaging a point source. Fluorescent particles can be considered point-like when the attenuation of their spectrum is negligible at the bandlimit of the microscope. This is only the case with objects of a size an order of magnitude smaller than the expected PSF size. Such objects usually offer a fluorescence signal too low for sufficient accuracy of measurement. Beads can be safely used when the shape of the bead spectrum is corrected for the attenuation (Van der Voort & Strasters, 1995). This is realized here by deconvolving the bead images with a bandwidth-limited object function assuming that the beads are uniformly dyed spheres. In the 4Pi-confocal case, the FWHM in the axial direction of the resulting PSF estimate was typically 10% narrower than the bead image.

Bead samples were prepared by placing a few drops of an undiluted suspension of red fluorescent beads (520/580 nm, excitation/fluorescence maximum; Molecular Probes, Oregon) of 115 nm diameter on a cover slip and dried. A few drops of Aquatex (Merck, Darmstadt) were added and then covered with another slip. Gentle pressing removed excess mountant so that a sample 10–15 μm thick was achieved. After 3–4 weeks the suspension became solid, with an index of refraction close to 1·5. As biological specimens we used mouse skin fibroblast cells embedded in a glycerol-based solution according to protocols described elsewhere (Bacallao *et al.*, 1990).

The restoration was based on a maximum-likelihood estimation (MLE) algorithm since it proved to be superior for low-intensity images (Van Kempen *et al.*, 1996). The solution found by the MLE algorithm was regularized by the method of Gaussian sieves. Here, a sieve with a sigma value of 0·2 sample interval was applied after each fifth iteration of the EM-MLE algorithm. The I-divergence of the imaged estimate and the recorded image was computed and compared to the value of the previous iteration of the algorithm. The iterations were stopped when the relative change of the I-divergence was below 0·01%.

Results

Figure 1 compares the resolution in confocal (a), restored confocal (b) and restored 4Pi-confocal (c) axial images of clustered beads. The images were taken consecutively in the same region of the specimen and are part of 3D data stacks consisting of 12 *xz*-slices with a pixel size of 44 nm and 20 nm in the *x*- and *z*-directions, respectively. The distance between the slices was 40 nm (*y*-direction) to ensure that the object was well sampled.

The two-photon confocal set-up (Fig. 1a) failed to resolve the beads. The beads also appear 3·5 times longer in the axial direction, and not spherical, as one would expect in a

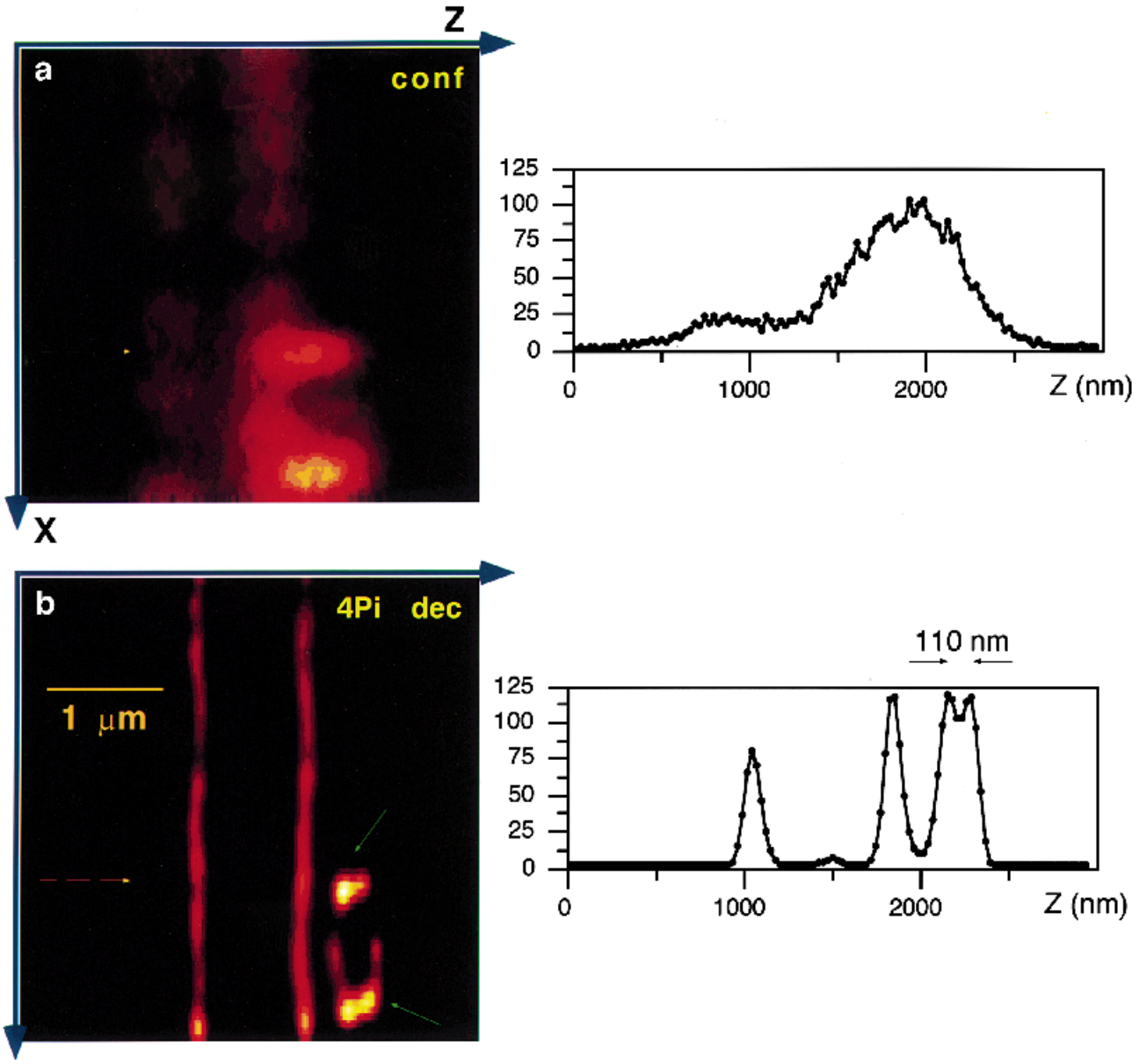

Fig. 3. Axial images of F-actin fibre bundles in a mouse skin fibroblast cell. While in the (a) confocal recording, the image is smeared by the poor axial resolution, the (b) restored 4Pi-confocal image resolves six distinct actin fibres (green arrows). The intensity profiles in the *z*-direction (dashed arrows) quantify the seven-fold improved axial resolution. The data stack consists of 20 layers taken at 40-nm steps in y. The improvement of lateral resolution in the cell is 1·5 fold, so that the total reduction of the measurement volume is by a factor of $(1{\cdot}5)^2{\cdot}7{\approx}15$.

faithful 3D image. The restoration with the confocal PSF improved the image slightly. However, the resolution remains nonisotropic so that beads closer than 300 nm to one another are not resolved. This is not the case in (c) where the 3D data have been collected using the 4Pi-confocal microscope and then restored with the 4Pi-PSF. In Fig. 1(c) the beads are unambiguously resolved. The lateral full-width-at-half-maximum (FWHM) of single restored bead images is 105 ± 10 nm; the axial FWHM is 70 ± 10 nm. In fact, the axial FWHM of the restored beads is slightly narrower (20 nm) than what one would expect from the bead object function. This could be explained by residual bead object information in the PSF which is practically unavoidable at the low light levels of fluorescence imaging. Thus the restoration of bead images results in restored beads that are slightly narrower. However, the resolution power of a microscope is judged on its ability to *distinguish* objects. This judgment is readily accomplished by evaluating data profiles of adjacent beads. Figure 2 exemplifies intensity profiles of beads at various distances,

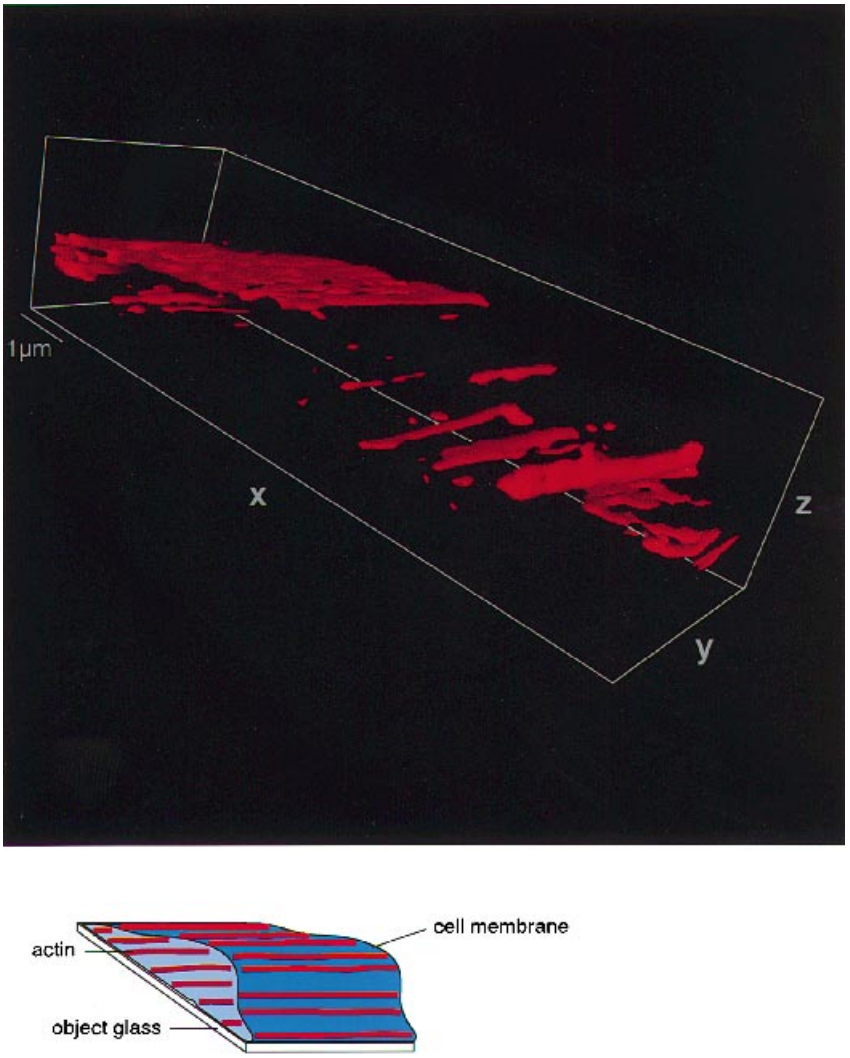

Fig. 4. Object-rendered 4Pi-confocal 3D image showing F-actin fibres and fibre bundles in a cross-section through the cell. The flat side reveals the area that is attached to the cover slip. The inset shows a scheme of the cell geometry. The image of the thin actin fibres features a FWHM of 85 nm in the axial and 200 nm in the lateral direction.

with Figs. 2(b) and (c) showing beads at close proximity. The profile of Fig. 2(c) represents two beads with an axial centre to centre distance of 120 nm, i.e. the beads were touching each other. A pronounced dip consisting of 5 pixels in the intensity profile can be observed, proving the 100 nm resolution of our system.

We applied our method to the imaging of labelled F-actin fibres of fibroblast cells (Fig. 3). The cells were mounted in a glycerol-based solution with a refractive index of 1·46, which is lower than that of the immersion oil and the coverslip (1·51). When scanning the sample in the *z*-direction, the optically denser medium is replaced by the thinner medium, so that the relative phase of the two wavefronts changes as a function of *z*. All indications so far are that this change is linear since the spherical wavefronts are primarily affected by the refractive index of the immersion system and the mountant. In the cytoskeleton the mountant represents more than 95% of the cell material. In our sample a complete turn of phase occurred after a 2·6-μm scan in the *z*-direction. The phase change is compensated for by a counteracting change in path lengths of one of the beams. This is achieved by applying a linear voltage ramp to a piezo-driven mirror in one of the illumination paths during the scan. Thus, it is possible to obtain an almost translation-invariant 3D 4Pi-confocal PSF in thicker specimens. As with a confocal microscope the maximum tolerable thickness is determined by the refractive index mismatch between the immersion system and the mountant (Hell *et al.*, 1993). For glycerol we estimate a tolerable thickness of 30–40 μm. Given a high sample transparency and an ideal match of refractive indices, the imaging of much thicker objects should be possible.

Figure 3 shows a confocal *xz*-image (a), together with the 4Pi-confocal restored counterpart (b). The axial images are part of a 3D data stack recorded in the cell cytoskeleton. Again, comparison of both methods reveals a fundamental improvement in resolution. We measured the FWHMs of various actin fibres or fibre bundles in the cell and found a

lateral FWHM of 280–330 nm in the confocal case, and 180–210 nm in the 4Pi-confocal restored case. Owing to the improved axial aperture of the 4Pi-confocal microscope, the increase in resolution is more prominent in the axial direction. In the confocal microscope we measure an axial FWHM of the cell actin fibres of 560–630 nm, whereas in its restored 4Pi-confocal counterpart a FWHM of 75–110 nm is observed.

The improvement in resolution is reflected in the fibres that can be distinguished. For example, an unresolved thick rod appears in the confocal data (Fig. 3a), suggesting a single, axially elongated fibre bundle. We note that this structure was not resolvable through restoration with the confocal PSF. However, in the 4Pi-confocal restored image the object is recognizable as distinct bundles of actin fibres. Finally, Fig. 4 shows a larger image of the F-actin in the fibroblast, which was obtained using the data of 20 *xz*-slices of a $4\times4\times10\,\mu$m volume.

Discussion and conclusion

Our method increases both the axial and the lateral resolution. Comparison with the confocal data reveals a reduction of the three-dimensional uncertainty volume up to a factor of 15. It is also apparent from the data that axial resolution is significantly better than lateral resolution. This can be explained by the fact that the 4Pi-confocal microscope doubles the aperture along the optic axis. Our approach holds promise for the investigation of transparent specimens whenever imaging with two high-aperture lenses is applicable, and the highest possible 3D resolution required. If the technique is performable at significant signal-to-noise ratio, further improvements are expected through applying shorter excitation wavelengths, i.e. 600 nm instead of the 810 nm used here.

Our 3D images of beads also indicate that for fluorescence spots, 3D resolution in the 75–100 nm range should be possible, thus providing an alternative to surface-bound near-field optics. Future research will concentrate on faster image acquisition (Juškaitis *et al.*, 1996), automated alignment, advanced restoration algorithms and application of the method to other parts of the cell, such as the nucleus. In the nucleus, we expect stronger changes of the refractive index, necessitating alteration of the phase compensation. This area of reserach is currently being investigated.

4Pi-microscopy provides the option of doubling the signal with respect to confocal or multiphoton microscopy through collection with both lenses. Here, we used only one lens for collection. However, the two-photon 4Pi-images feature a signal that is on average approximately three times higher. The reason is that a higher local intensity is achieved with the sharper focus, in conjunction with the higher order dependence of excitation on intensity. Thus, 4Pi-confocal microscopy provides efficient multiphoton excitation and high sensitivity. In a synergistic combination with restoration techniques, this method results in what is, to our knowledge, the highest three-dimensional resolution in light microscopy at present.

Acknowledgments

We gratefully acknowledge the preparation of the fibroblast cell sample by G. Giese and co-workers (Max-Planck-Institute for Cell Biology, Ladenburg, Germany).

References

Abbe, E. (1873) Beiträge zur Theorie des Mikroskops und der mikroskopischen Wahrnehmung. *Archive f. Mikroskop. Anat.* **9**, 413–420.

Agard, D.A. & Sedat, J.W. (1983) Three-dimensional architecture of a polytene nucleus. *Nature*, **302,** 676–681.

Bacallao, R., Bomsel, M., Stelzer, E. & de Mey, J. (1990) Guiding principles of specimen preservation for confocal fluorescence microscopy. *Handbook of Biological Confocal Microscopy* (ed. by J. B. Pawley), pp. 197–205. Plenum Press, New York.

Bailey, B., Farkas, D.L., Taylor, D.L. & Lanni, F. (1993) Enhancement of axial resolution in fluorescence microscopy by standing-wave excitation. *Nature*, **366**, 44–48.

Carrington, W.A., Lynch, R.M., Moore, E.D.W., Isenberg, G., Fogarty, K.E. & Fay, F.S. (1995) Superresolution in three-dimensional images of fluorescence in cells with minimal light exposure. *Science*, **268,** 1483–1487.

Castleman, K.R. (1979) *Digital Image Processing*. Prentice-Hall, Englewood Cliffs, NJ.

Denk, W., Strickler, J.H. & Webb, W.W. (1990) Two-photon laser scanning fluorescence microscopy. *Science*, **248,** 73–76.

Hell, S.W. (1990) Double-scanning confocal microscope. *EP0491289* (filed, 1990, published, 1992).

Hell, S.W. (1994) Improvement of lateral resolution in far-field light microscopy using two-photon excitation with offset beams. *Opt. Commun.* **106,** 19–22.

Hell, S.W., Bahlmann, K., Schrader, M., Soini, A., Malak, H., Gryczynski, I. & Lakowicz, J.R. (1996) Three-photon excitation in fluorescence microscopy. *J. Biomed. Opt.* **1,** 71–73.

Hell, S., Reiner, G., Cremer, C. & Stelzer, E. (1993) Refractive index mismatch induced aberrations in confocal fluorescence microscopy. *J. Microsc.* **169,** 391–405.

Hell, S. & Stelzer, E.H.K. (1992) Fundamental improvement of resolution with a 4Pi-confocal fluorescence microscope using two-photon excitation. *Opt. Commun.*, **93,** 277–282.

Hell, S.W. & Wichmann, J. (1994) Breaking the diffraction resolution limit by stimulated emission. *Opt. Lett.* **19,** 780–782.

Juškaitis, R., Wilson, T., Neil, M.A.A. & Kozubek, M. (1996) Efficient real -time confocal microscopy with white light sources. *Nature*, **383,** 804–806.

Kano, H., van der Voort, H.T.M., Schrader, M., van Kempen, G.M.P. & Hell, S.W. (1996) Avalanche photodiode detection with object scanning and image restoration provides 2–4 fold resolution increase in two-photon fluorescence microscopy. *Bioimaging*, **4,** 187–197.

Marti, O. & Amrein, M. (1993) *STM and SFM in Biology.* Academic Press, New York.

Müller, M. & Brakenhoff, G.J. (1996) Using offset interfering beams for improved resolution in confocal imaging: the potential of the PSAF-technique. *Bioimaging*, **4,** 179–186.

Schrader, M., Bahlmann, K. & Hell, S.W. (1997) Three-photon excitation microscopy: theory, experiment and applications. *Optik*, **104,** 116–124.

Schrader, M. & Hell, S.W. (1996) 4Pi-confocal images with axial superresolution. *J. Microsc.* **183,** 189–193.

Schrader, M., Hell, S.W. & Van der Voort, H.T.M. (1996) Potential of confocal microscopes to resolve in the 50–100 nm range. *Appl. Phys. Lett.* **69,** 3644–3646.

Sheppard, C.J.R. (1995) Fundamental reduction of the observation volume in far-field light microscopy by detection orthogonal to the illumination axis:Confocal theta microscopy-comment. *Opt. Commun.* **119,** 693–694.

Stelzer, E.H.K. & Lindek, S. (1994) Fundamental reduction of the observation volume in far-field light microscopy by detection orthogonal to the illumination axis: confocal theta microscopy. *Opt. Commun.*, **111,** 536–547.

Vaez-Iravani, M. & Kavaldjiev, D.I. (1995) Resolution beyond the diffraction limit using frequency-domain field confinement in scanning microscopy. *Ultramicroscopy*, **61,** 105–110.

Van der Voort, H.T.M. & Strasters, K.C. (1995) Restoration of confocal images for quantitative analysis. *J. Microsc.* **178,** 165–181.

Van Kempen, G.M.P., van der Voort, H.T.M., Bauman, J.G.J. & Strasters, K.C. (1996) Comparing maximum likelihood estimation and constrained Tikhonov-Miller restoration. *IEEE Eng. Med. Biol.* 76–83.

Wilson, T. (1990) *Confocal Microscopy*, pp. 27–32. Academic Press, London.

Wokosin, D.L., Centonze, V.E., Crittenden, S. & White, J. (1996) Three-photon excitation fluorescence imaging of biological specimens using an all-solid-state laser. *Bioimaging*, **4,** 208–214.